Geomechanics and Engineering, *Vol. 13, No. 6 (2017) 977-995*
DOI: https://doi.org/10.12989/gae.2017.13.6.977

The investigation of rock cutting simulation based on discrete element method

Xiaohua Zhu[*1], Weiji Liu[**1] and Yanxin Lv[1,2]

[1]*School of Mechatronic Engineering, Southwest Petroleum University, Chengdu 610500, China*
[2]*State Key Laboratory of Geomechanics and Geotechnical Engineering, Institute of Rock and Soil Mechanics, Chinese Academy of Sciences, Wuhan 430071, China*

(Received January 7, 2016, Revised May 29, 2017, Accepted June 16, 2017)

Abstract. It is well accepted that rock failure mechanism influence the cutting efficiency and determination of optimum cutting parameters. In this paper, an attempt was made to research the factors that affect the failure mechanism based on discrete element method (DEM). The influences of cutting depth, hydrostatic pressure, cutting velocity, back rake angle and joint set on failure mechanism in rock-cutting are researched by PFC2D. The results show that: the ductile failure occurs at shallow cutting depths, the brittle failure occurs as the depth of cut increases beyond a threshold value. The mean cutting forces have a linear related to the cutting depth if the cutting action is dominated by the ductile mode, however, the mean cutting forces are deviate from the linear relationship while the cutting action is dominated by the brittle mode. The failure mechanism changes from brittle mode with larger chips under atmospheric conditions, to ductile mode with crushed chips under hydrostatic conditions. As the cutting velocity increases, a grow number of micro-cracks are initiated around the cutter and the volume of the chipped fragmentation is decreasing correspondingly. The crack initiates and propagates parallel to the free surface with a smaller rake angle, but with the rake angle increases, the direction of crack initiation and propagation is changed to towards the intact rock. The existence of joint set have significant influence on crack initiation and propagation, it makes the crack prone to propagate along the joint.

Keywords: discrete element method; rock cutting; failure mechanism; fracture propagation; hydrostatic pressure

1. Introduction

Mechanical rock cutting is widely encountered in petroleum engineering, such as oil gas drilling (Franca and Lamine 2010). The understanding of rock cutting processes could be very useful in designing rock cutting tools and determining optimum rock cutting process parameters (Menezes *et al.* 2014). There have two approaches which are commonly used to research the rock cutting mechanism, one is the laboratory test and the other is numerical simulation. Although the laboratory test can obtain a reliable result, it is generally time-consuming and also a waste of

*Corresponding author, Professor, E-mail: zxhth113@163.com
**Corresponding author, Ph.D., E-mail: lwjzq1111@163.com

Copyright © 2017 Techno-Press, Ltd.
http://www.techno-press.org/?journal=gae&subpage=7 ISSN: 2005-307X (Print), 2092-6219 (Online)

money. On the contrary, the numerical simulation can provide a faster and cheaper way. There are a lots of numerical simulation researches about rock cutting based on finite element method (FEM) (Fang and Harrison 2002, Innaurato *et al.* 2007, Onate and Rojek 2004, Menezes *et al.* 2014, Fontoura *et al.* 2012), but in many researches, the chip formation is only modeled without dealing with the post failure behavior. The DEM, which is used in this study, allows the simulation of damage, chip formation and crack initiation, propagation and coalescence (Rojek *et al.* 2011, Ledgerwood 2007, Su and Akcin 2011, He and Xu 2015, Xu *et al.* 2015).

Molecular dynamics based DEM simulations of indentation and cutting processes at the nanoscale were first reported in (Hoover *et al.* 1990, Shimada and Ikawa 1998). The feasibility of using the DEM to investigate the rock cutting process was explored in (Huang *et al.* 1999, Lei and Kaitkay 2003, Onate and Rojek 2004, Stavropoulou 2006, Block and Jin 2009, Mendoza *et al.* 2010, Rojek *et al.* 2011, Mendoza *et al.* 2011). The dynamic response mechanism of the rock fragmentation and its influential factors have been researched based on the particle flow code, the results show that the rock fragmentation process is composed of the cycle of various small shearings and on large shearing (Tan *et al.* 2013). The effect of downhole conditions on cutting morphology was investigated by using the two-dimensional DEM (Block and Jin 2009). He and Xu (2015) has made an attempt to model rock cutting process and to check the dependence of the critical failure mode transition depth on the brittleness of rock; the results demonstrate that failure mode transition took place both in clustered model and non-clustered model, but for the clustered model the transition emerged at a shallower cutting depth. Huang (2013) has conducted the numerical simulations of the cutting process to reproduce the transition from a ductile to a brittle failure mode with increasing depth of cut. The numerical results provide evidence that the critical depth of cut controlling the failure mode transition is related to the characteristic length. Richard *et al.* (1998, 1999) used an experimental method to assess the strength of sedimentary rocks and the testing procedure and some experimental results are described, the experimental show that the failure modes in rock cutting can be divided into two. One is ductile failure (Fig. 1(a)) occurring at a small cutting depth, characterized by a continuous plastic flow of crushed materials ahead of the cutting tool. The other one is brittle failure (Fig. 1(b)) occurring when the cutting depth increases beyond a threshold value, characterized by the initiation and propagation of macroscopic cracks along the horizontal direction.

It is well known that there is a transition of failure mode from ductile to brittle with increasing depth of cut during rock cutting process. Whether there have some other factors influence the failure mechanism? This is a very interesting question. Compared with the rock cutting simulations before, the present model is simulated as a hydrostatic pressure applied on the rock surface and the joint set is considered, which we believe to be an innovation of rock cutting simulation. The effects of cutting depth, hydrostatic pressure, cutting velocity, back rake angle and joint set on failure mechanism are researched.

(a) Ductile mode at a depth of cut d=1 mm

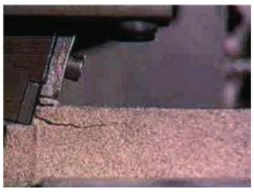

(b) A brittle mode at a depth of cut d=4 mm

Fig. 1 The failure mode in rock cutting (Richard 1999)

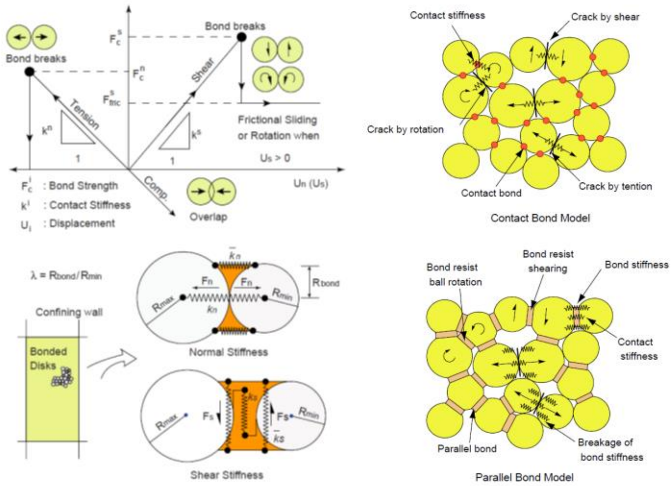

Fig. 2 Illustration of bond models provided in PFC (Cho *et al.* 2007)

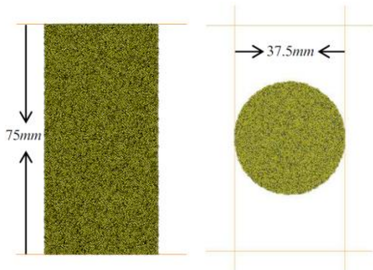

Fig. 3 Two-dimensional numerical specimens for UCS and BTS tests

2. Determination of rock model parameters

PFC is used to simulate the mechanical behavior of rock by considering the system as a collection of separate particles bonded together at their contact points, widely used to solve many rock engineering and geo-mechanics problems. A major challenge using PFC is selecting the necessary micro-mechanical parameters of particles and bonds that result in representative intact rock properties. Several combinations of different micro-mechanical properties can result in similar macroscopic mechanical properties (Lichun *et al.* 2013).

PFC provides two standard bonding behaviors: named contact bonds (CB) and parallel bonds (PB). Both bonds can be envisioned as a kind of glue joining the two particles. The contact-bond glue is of a vanishingly small size that acts only at the contact point, while the parallel-bond glue is of a finite size that acts over either a circular or rectangular cross-section lying between the particles. The contact bond can transmit only a force, while the parallel bond can transmit both a force and a moment (Itasca 2002). In CB model, the contact stiffness is still active even after bond breakage as long as particle contact is maintained, which mean that the breakage of bond cannot significantly influence the macro stiffness in CB model. This property of CB model is different to the real rocks to some extent. In the PB model, however, stiffness is contributed by both contact stiffness and bond stiffness. Thus, bond breakage in the PB model, immediately results in stiffness reduction, which not only affects the stiffness of adjacent assemblies but also affects the macro stiffness of the particle assemblage (Cho *et al*. 2007). These features of CB and PB are also illustrated in Fig. 2. As the above state the PB model is a more realistic bond model for rock-like than the CB model. For this reason, the PB model was selected in this paper.

PFC simulations require proper selection of micro-parameters by means of calibration processes in which the responses of the numerical model are compared directly to the observed responses of the physical material (Pradeep *et al.* 2014). The most important mechanical properties of the rock include the Young's modulus E, Poisson's coefficient υ, compressive strength σ_c and tensile strength σ_t. These properties will be used in calibrating the micro-properties of the model (Ghazvinian *et al.* 2014).

Young's modulus, uniaxial compressive strength and Poisson's ratio are normally obtained by the simulation of unconfined compression test and the tensile strength derived by the simulation of the indirect tension (Brazilian) test. The diameter and height of the specimen are 37.5 mm and 75 mm, respectively. Compaction of the particle assembly has been characterized by a porosity of 17%. The cylindrical specimen of the diameter 37.5 mm for the simulation of the BTS test has been obtained by trimming adequately the specimen used in the UCS simulation. Sketch of PFC rock models are illustrated in Fig. 3.

2.1 Parametric study on macro-mechanical parameters

Unlike continuum-based numerical codes such as FEM where the macro-mechanical properties of the specimen can be directly specified, DEM suffers from the disadvantage of an additional numerical calibration procedure, i.e., the determination of micro-scale parameters given a set of macro-mechanical properties, such as Young's modulus E, Poisson's ratio υ, uniaxial compressive strength σ_c and tensile strength σ_t.

Table 1 Results of UCS and BTS tests with varying parallel bond modulus

pb_EC (GPa)	E (GPa)	υ	σ_c (MPa)	σ_t (MPa)	σ_c/σ_t
3	3.5	0.279	141	26.8	5.26
13	14.5	0.287	120	23.3	5.15
23	25.7	0.289	126	30.5	4.13
33	37	0.288	126	27.1	4.65
43	47.6	0.283	119	28.2	4.22
53	57	0.282	115	27.4	4.19
63	67	0.285	109	30.2	3.6
73	81	0.28	124	30	4.1
83	90	0.286	114	27.4	4.16

Table 2 Results of UCS and BTS tests with varying ratio of parallel bond normal to shear stiffness

pb_krat	E (GPa)	υ	σ_c (MPa)	σ_t (MPa)	σ_c/σ_t
0.5	157	0	108.6	25.4	4.27
0.7	145.6	0.047	110	27.7	3.97
1	138.6	0.12	105	26.7	3.93

Table 2 Continued

pb_krat	E (GPa)	υ	σ_c (MPa)	σ_t (MPa)	σ_c/σ_t
1.2	128.6	0.13	107.3	25.9	4.1
1.5	121.9	0.17	115.2	37.2	3.1
1.7	121.3	0.184	125.5	26.6	4.7
2.5	106.8	0.24	131.4	22.2	5.9
3	97	0.246	115.5	27.1	4.26
5	82.9	0.31	111.4	26.3	4.2
10	54.6	0.36	100.9	21	4.8

Table 3 Results of UCS and BTS tests with varying normal strength

pb_sn (MPa)	E (GPa)	υ	σ_c (MPa)	σ_t (MPa)	σ_c/σ_t
31	90	0.28	41.8	7.8	5.35
36	88.9	0.28	47.3	11.4	4.15
41	89	0.277	50.4	12.6	4
51	90	0.28	62	14.5	4.27
61	89	0.284	74.4	15.2	4.9
71	89.8	0.29	91.2	20.7	4.4
81	89.9	0.286	105.4	24.7	4.26
91	90	0.285	114	27.4	4.16
101	90.1	0.28	126.7	30.5	4.15

Table 4 Results of UCS and BTS tests with varying shear strength

pb_ss (MPa)	E (GPa)	υ	σ_c (MPa)	σ_t (MPa)	σ_c/σ_t
31	87	0.289	59.3	11.9	4.98
36	87.3	0.285	63.7	17.6	3.62
41	88	0.282	73.2	21	3.5
51	89.8	0.286	83.9	20.8	4.03
61	89.7	0.28	84	21.7	3.87
71	90	0.279	100.9	25	4.03
81	90	0.278	110	27.1	4.05
91	90	0.279	114	27.4	4.16
101	90	0.28	119	27.5	4.33

2.1.1 Effect of parallel bond modulus

The influence of parallel bond modulus on macro-mechanical parameters is presented in Table 1. It shows that the Young's modulus increases with the parallel bond modulus (pb_EC), but parallel bond modulus has little effect on Poisson's ratio, uniaxial compressive strength σ_c and tensile strength σ_t and its ratio of σ_c/σ_t.

2.1.2 Effect of the ratio of parallel bond normal to shear stiffness

Diederich (2000) and Potyondy and Cundall (2004) showed that the contact normal to shear stiffness ratio (pb_krat) involves Poisson's ratio. The Passion's ratio increases with the stiffness ratio. In this study, the ratio of parallel bond normal to shear stiffness is changing in the range of 0.5 to 10. Table 2 reveals that the Young's modulus decreases with the stiffness ratio, and the stiffness ratio has little influence on uniaxial compressive strength σ_c and tensile strength σ_t and its ratio of σ_c/σ_t.

(a) (b)

Fig. 4 Microscal failure of particle assemble under uniaxial compression

Table 5 Micro-properties for rock sample

ρ (kg/m^3)	ba_Ec (GPa)	ba_Frat	ba_Fric	Pb_Rmult	pb_sn (MPa)	pb_ss (MPa)
2620	28	3.8	0.5	1	91±20	91±20

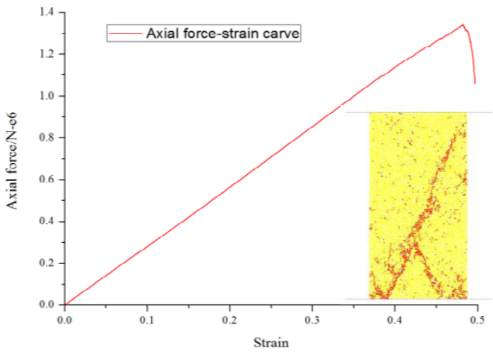

Fig. 5 Axial stress versus axial strain and cracks of the UCS test

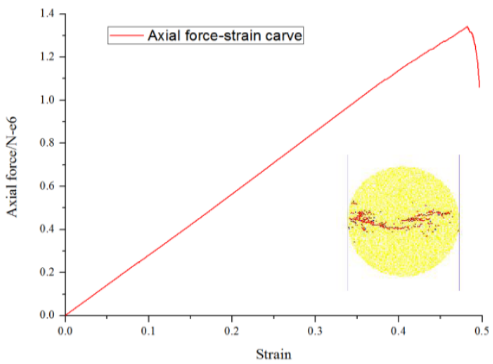

Fig. 6 Axial force versus axial strain and cracks of the BTS test

Table 6 Macro-properties for rock sample

E (GPa)	υ	σ_c (MPa)	σ_t (MPa)	σ_c/σ_t
32	0.28	121	22.4	4.16

2.1.3 Effect of bond strength

In PFC, the micro-strengths must be iteratively selected to match the macro-scale strength. The most important parameters that characterize the macro-strength and micro-fracture behavior are the parallel bond normal (pb_sn) and shear strength (pb_ss) and its ratio. As shown in Tables 3 and 4, the uniaxial compressive strength σ_c and tensile strength σ_t increase with the normal and shear strength, the normal and shear strength have little influence on the Young's modulus, Poisson's ratio and the ratio of σ_c/σ_t.

Among all these factors, the bond strength ratio σ_c/σ_t is the critical parameter controlling the microscale failure mechanism. By increasing this ratio, the microscale failure evolves from a tensile dominant to a shear dominant mode. Just illustrated in Fig. 4, which shows the microscale failure pattern of a discrete particle system under uniaxial compression for σ_c/σ_t=0.1 and 10. For σ_c/σ_t=0.1, all the particle bonds are breaking in tensile (Fig. 4(a)). For σ_c/σ_t=10, the microscale failure mechanism tends to be breaking in shear (Fig. 4(b)).

The micro-properties of rock sample selected in this paper are shown in Table 5.

The UCS and BTS tests are performed to calibrate the relations between micro-properties and mechanical properties of the rock specimens, just as Figs. 5 and 6. The stress-strain curve and failure mode of the UCS test are shown as Fig. 5. Uniaxial compressive strength σ_c, young's modulus E, Poisson's ratio υ can be calculated from the stress-strain curve of UCS. Simulation result of the BTS test is presented in Fig. 6. The tensile strength σ_t can be calculated from the stress-strain curve of BTS. The obtained macro-properties of rock specimens are presented in Table 6.

3. Numerical model of rock cutting

The rock cutting model as the Fig. 7 shows is consisting of a cutter and a rock sample of the size 20 mm×40 mm. The rock specimen is composed of 26,635 balls of radius in the range of 0.075 mm-0.1125 mm. The average radius of balls is represented by R. The rectangular specimen is confined by three frictionless walls on the bottom, left and right sides. The cutter is moved horizontally across the rock at a constant velocity of V with a back-rake angle α and at a fixed cutting depth d. The tool-rock interaction is modeled by the coulomb friction model. The cutter is moved horizontally across the rock at a relatively low velocity to ensure quasi-static equilibrium state of the assembly.

Drilling mud is a viscous liquid that cannot sustain shear stress; thus, the load it provides to the rock surface can be characterized by a pressure. However, in the actual drilling process, the rock not only suffers the drilling mud pressure but suffers the high pore pressure. In this paper, the pressure apply on the rock surface is equal to the difference between drilling mud pressure and pore pressure, what is more, the balanced and overbalanced drilling situation are only considered.

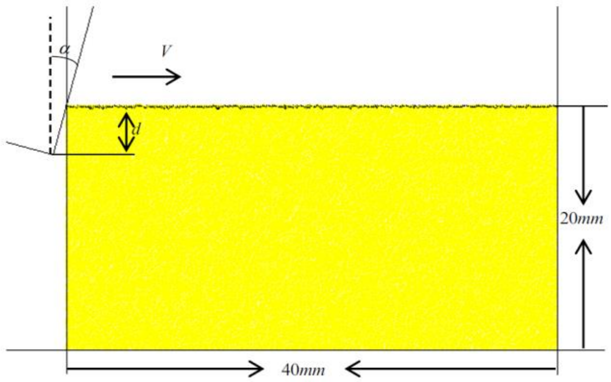

Fig. 7 Schematic illustration of rock cutting

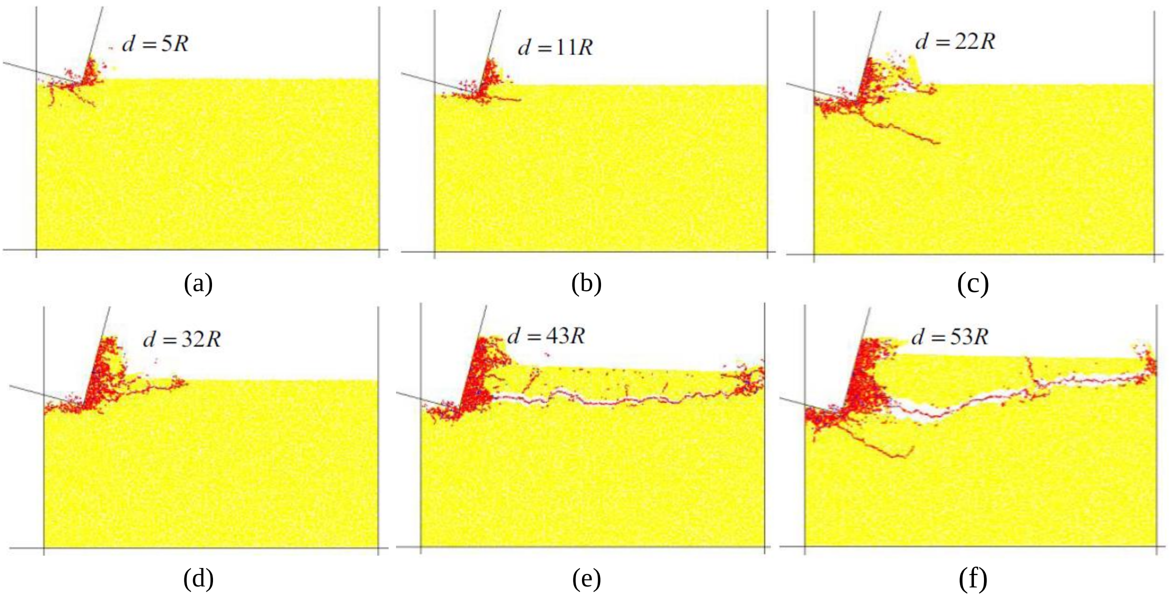

Fig. 8 Fracture evolution of rock cutting with various cutting depths under atmospheric pressure

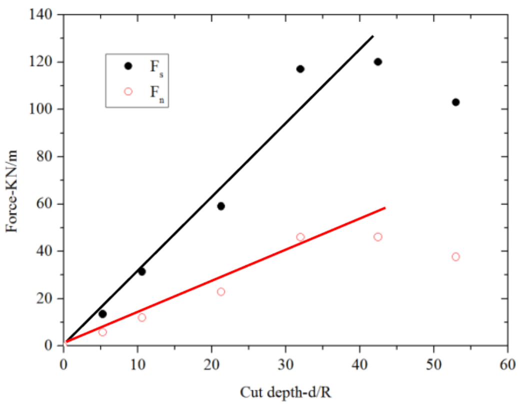

Fig. 9 Average cutting forces with various cutting depths under atmospheric pressure

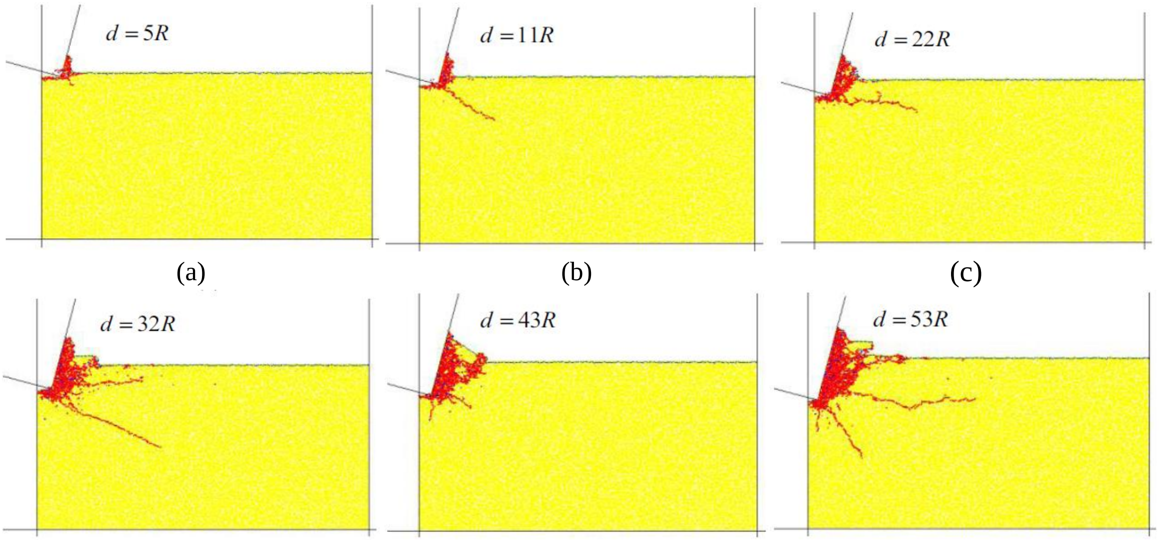

Fig. 10 Fracture evolution of rock cutting with various cutting depths under hydrostatic pressure

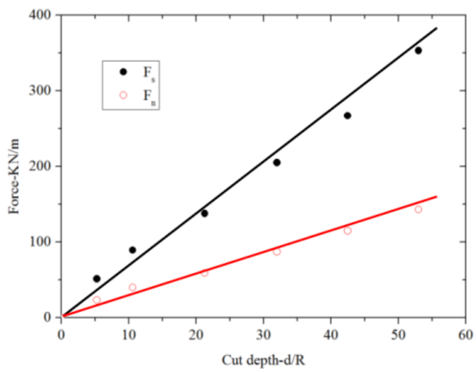

Fig. 11 Average cutting forces with various cutting depths under hydrostatic pressure

4. The effect of cutting depth on rock cutting

4.1 Under atmospheric pressure condition

The horizontal cutting velocity is 0.5 m/s, the cutting velocity is so small that the rock is considered to be in a quasi-static condition. The fracture evolution during the cutting process is clearly presented in Fig. 8. The cutting depths of (a), (b), (c), (d), (e), (f) are 5*R*, 11*R*, 22*R*, 32*R*, 43*R*, 53*R* respectively. The ductile failure occurs at shallow cutting depths, characterized by a continuous plastic flow of crushed materials ahead of the cutting tool. The brittle failure occurs as the depth of cut increases beyond a threshold value, characterized by the initiation and propagation of macroscopic cracks along the horizontal direction.

The cutting mode transition can also be described by the average cutting forces. The mean forces should have a linear related to the cutting depth if the cutting action is dominated by the ductile mode. However, the mean cutting forces tend to deviate from the linear relationship while the brittle mode is dominated. Just as Fig. 9 shows, the mean cutting forces keep increasing linearly until about d/R=33. While d/R>33, it shows a non-linear relationship, representing the rock failure mode changes.

4.2 Under hydrostatic pressure condition

The fracture evolution during the cutting process with hydrostatic pressure 5MPa is clearly presented in Fig. 10. The cutting depths of 10(a), 10(b), 10(c), 10(d), 10(e), 10(f) are 5*R*, 11*R*, 22*R*, 32*R*, 43*R*, 53*R* respectively. The mean cutting forces with various cutting depth under hydrostatic pressure are shown in Fig. 11. From Figs. 10 and 11, we know that the hydrostatic pressure could significantly influence the fracture evolution, inhibiting the formation of the long horizontal fracture. Even the cutting depth is *d*=53*R*, the failure mode is dominated by ductile failure. As shown in Fig. 11, the mean cutting forces always keep increasing linearly until d/R=53 or even larger. The larger cutting depths cases are not calculated in this paper.

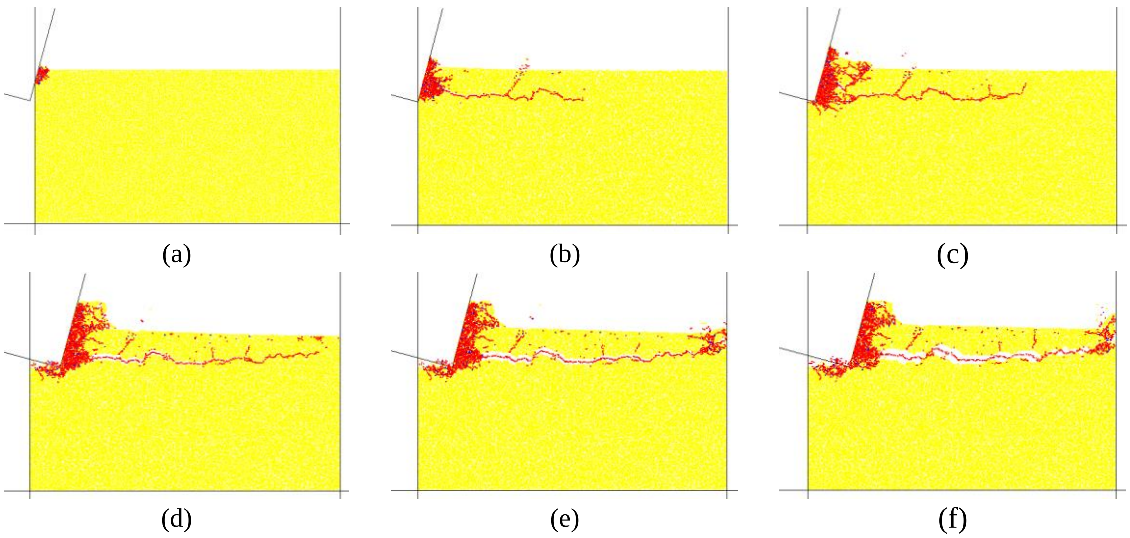

Fig. 12 Fracture evolution of rock cutting with atmospheric pressure

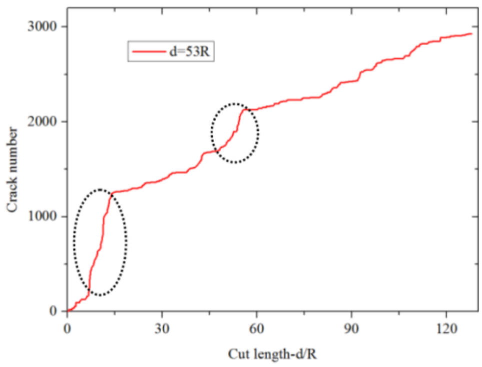

Fig. 13 The crack number versus cut length under atmospheric pressure

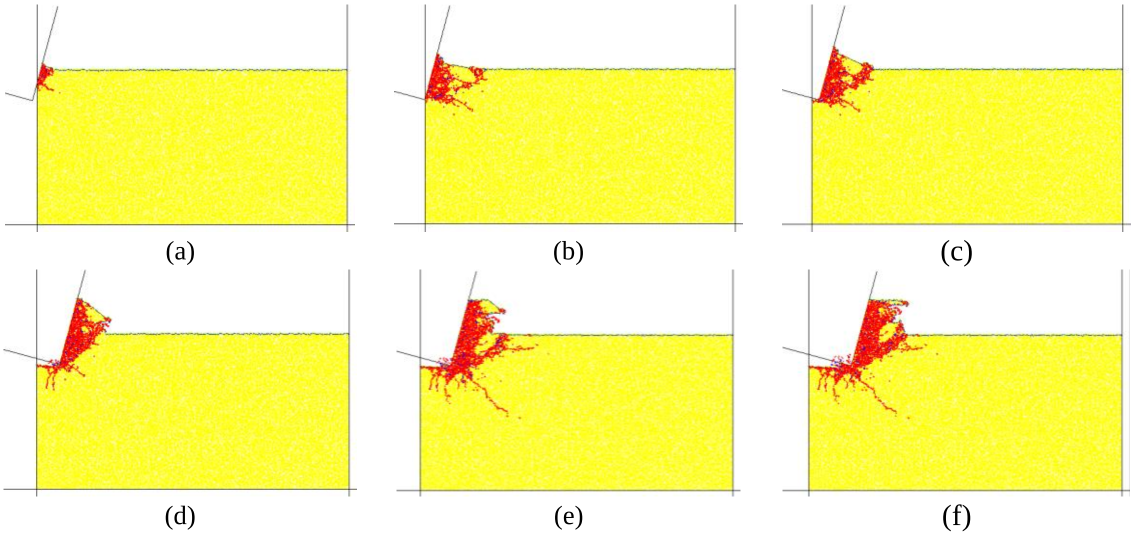

Fig. 14 Fracture evolution of rock cutting with hydrostatic pressure

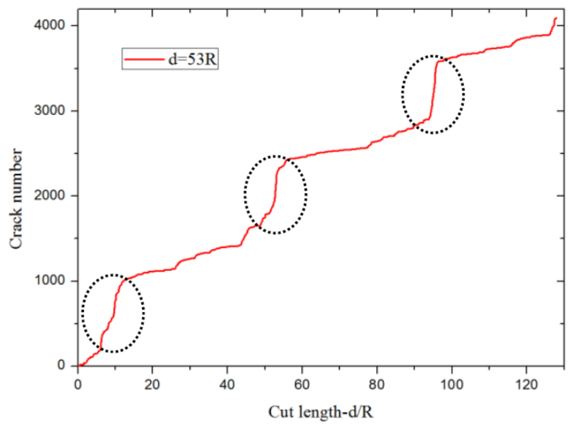

Fig. 15 The crack number versus cut length under hydrostatic pressure

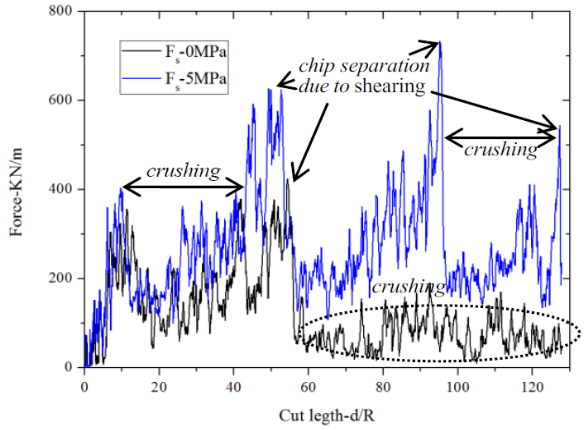

Fig. 16 Cutting force under atmospheric and hydrostatic pressure

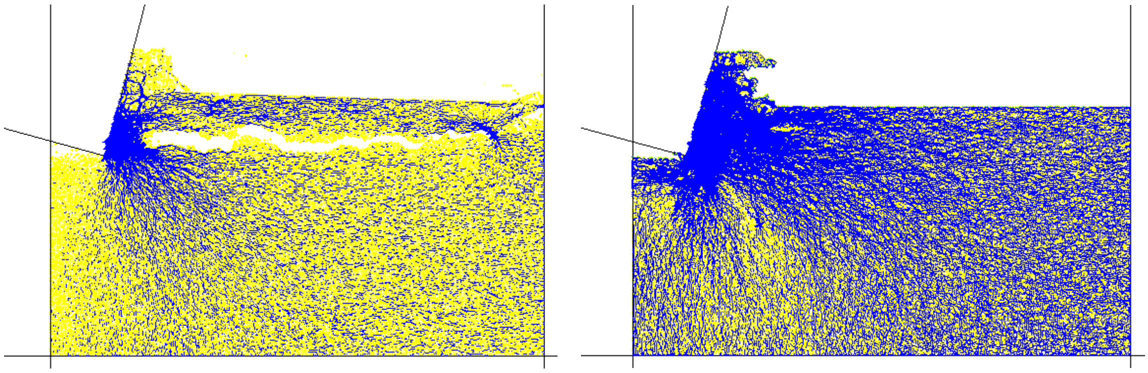

(a) (b)

Fig. 17 Contact force in brittle and ductile modle (blue lines)

5. The effect of hydrostatic pressure on rock cutting

In actual drilling process, the bottom rock may under balanced, underbalanced or overbalanced situation while under the combined action of drilling mud pressure and pore pressure. The balanced situation formed when the drilling pressure is equal to the pore pressure and the underbalanced and overbalanced situation formed while the drilling pressure is lower and larger than the pore pressure respectively. In order to make clear the effect of hydrostatic pressure on failure mechanism, the balanced (atmospheric pressure) and overbalanced (hydrostatic pressure) situations are researched in this paper.

5.1 Fracture evolution of rock cutting under atmospheric pressure condition

The horizontal cutting velocity is 0.5 m/s and the depth of cut is 4 mm. The fracture evolution during the cutting process is presented in Fig. 12. The crack number is shown in Fig. 13.

It is well known that a zone of highly fractured and deformed rock is created beneath the cutter (Cundall and Hart 1985). Underneath the indenter there is a crushed zone and a cracked zone. The sizes of the crushed zone and the cracked zone, and the lengths of various kinds of cracks are mainly dependent on the magnitude of load, the mechanical properties of the rock and the geometry of the indenter as well (Mahabadi *et al.* 2012).

As can be seen from the fracture evolution, splitting of chips typical for brittle rock cutting has been reproduced in numerical simulation, similar to those observed in reported experiments for rock cutting. As the cutter acts on the rock, a highly stressed zone comes into being immediately. The pressurised zone is contributed to the formation of the crushed zone. The crushed zone starts to form at a relatively small penetration and the damaged rock undergoes some volume dilation that causes extra expansion to the surrounding rock and stimulates the indentation cracking. There are chipping cracks and subsurface cracks in the case of rock cutting with no hydrostatic pressure. The fractures in the upper area developed rather quickly into the rock along the horizontal direction. The horizontal crack could eventually arrive at the free surface, thus causing a large volume of fragment chips. The chips were formed with the development of the long horizontal fracture. The subsurface fractures are actually the bifurcation of some major tensile fractures during the cutting process. It is confirmed that the numerical model could successfully simulate the process of chip formation, contributing to an improved knowledge of the rock fragmentation process.

5.2 Fracture evolution of rock cutting under hydrostatic pressure condition

In order to investigate the influence of hydrostatic pressure on rock cutting, we carry out rock cutting simulation with a pressure of 5 MPa acting on the rock surface, with a cutting depth of 4 mm, and rock cutting velocity of 0.5 m/s. The number of the crack increases as the hydrostatic pressure increases, as presented in Figs. 13 and 15. It can be noticed that high hydrostatic pressure could promote the development of the crack, increasing the energy requirements of drilling and effectively strengthening the rock.

Comparing the fracture evolution mode with no hydrostatic pressure, it can be easily observed that hydrostatic pressure could significantly influence the fracture evolution, inhibiting the formation of the long horizontal fracture. The failure mechanism changes from brittle mode with larger chips under atmospheric conditions, to ductile mode with crushed chips under hydrostatic conditions, just as Fig. 14 shows. The carve shows rapid increase in number of cracks regularly in the cutting processes as the black-dotted circles marked in Fig. 15. These sudden increases in micro-fractures are indications of the crushed zone adhering to the tip of the cutter and cutting chip formations. The volume of the cutting chips is smaller compared with that cutting with no surface pressure.

Force responses are regarded as the most significant and straightforward factor for indicating tool performance and process limitations and are also commonly considered as being the best indicators in evaluating the accuracy of numerical simulation methods. Chip formation and material removal phenomena are the primary factors that affect the cutting force responses in rock cutting (Chen *et al.* 2014).

Therefore, great efforts have been made to get a reliable result of cutting force. The cutting force carves, under atmospheric pressure and hydrostatic pressure conditions are shown in Fig. 16. As shown in the figure, the cutting force of hydrostatic pressure is relatively larger than the atmospheric pressure. For the atmospheric pressure cutting case, the cutting force shows sudden decrease when the cutting length reach about 55R and keeps a low level in the later long cutting length as the black-dotted circles marked in Fig. 16. It is because the cracks have propagated towards the free surface leads eventually to rock chipping and fragmentation due to the shearing mechanisms. But for the hydrostatic pressure case, the cutting force also shows the phenomenon of sudden decrease, while it will increase in the later cutting process and this phenomenon will occur in an alternating manner. As shown in Fig. 16, there are several peaks and valleys of cutting force which monitored during the cutting simulation. The higher force magnitudes imply a higher surface energy status of rock. When the cutting force reaches a certain value, a relatively big chip will be formed and then separate from the main rock, which leads to a sudden decrease of the cutting force magnitude. The crushing mechanism occurs after the separation of chips with small variations and relatively small magnitude cutting force magnitude. As stated above, the shearing and crushing mechanisms are occurring in an alternating manner. Comparing to Figs. 13 and 14, the cutting force sudden decreases with the crack number sudden increases.

The contact force is shown in Fig. 17. The rock sample fails in brittle mode as shown in Fig. 17(a) and fails in ductile mode as shown in Fig. 17(b). The contact forces between particles are more localized near the tip of the cutter in brittle mode than in ductile mode.

6. The effect of cutting velocity on rock cutting

The effects of cutting velocity on mechanism are shown in Figs. 18 and 19. Fig. 18 represents the cases with atmospheric pressure and Fig. 19 represents the cases with hydrostatic pressure. The cutting velocity is 0.1 m/s, 0.5 m/s and 1 m/s respectively. From the figures we know the failure mode transition from brittle mode to ductile mode while the cutting velocity increasing from 0.1 m/s to 1 m/s. As the cutting velocity increases, the more and more micro-cracks are initiated around the cutter and the volume of the chipped fragmentation is decreasing correspondingly. As shown in Figs. 20 and 21, the crack number increases with the cutting velocity increases and the increased numbers of crack almost occurred the front of the tip of cutter.

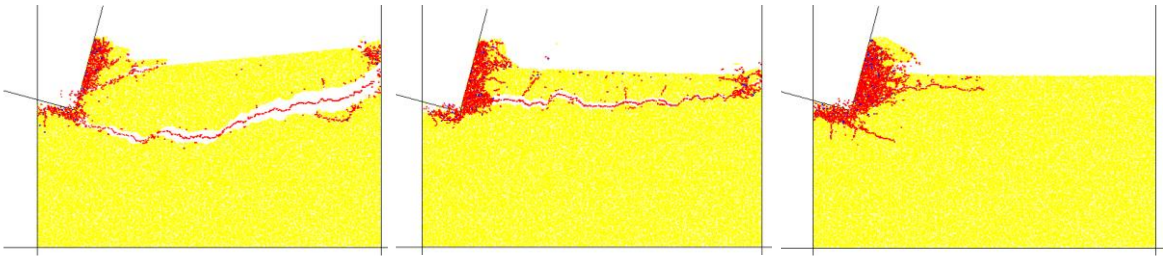

(a) (b) (c)

Fig. 18 Failure mechanism under atmospheric pressure with various cutting velocity

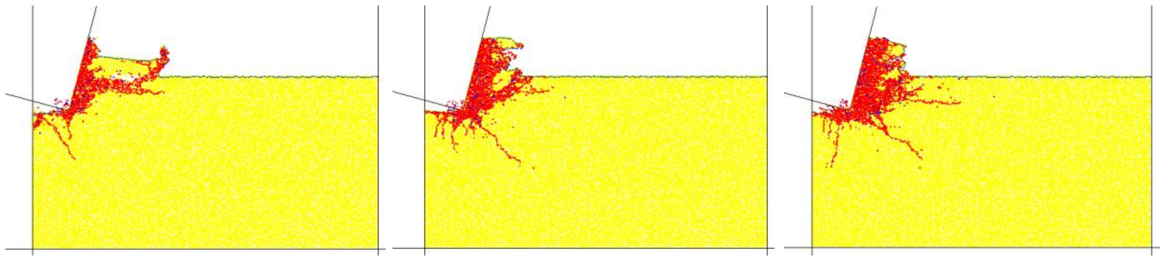

(a) (b) (c)

Fig. 19 Failure mechanism under hydrostatic pressure with various cutting velocity

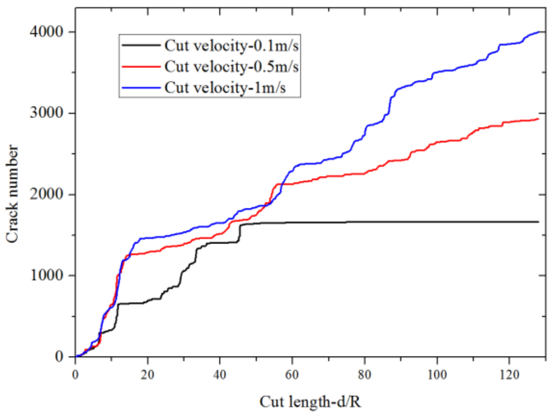

Fig. 20 Crack number versus cut length under atmospheric pressure with various cutting velocity

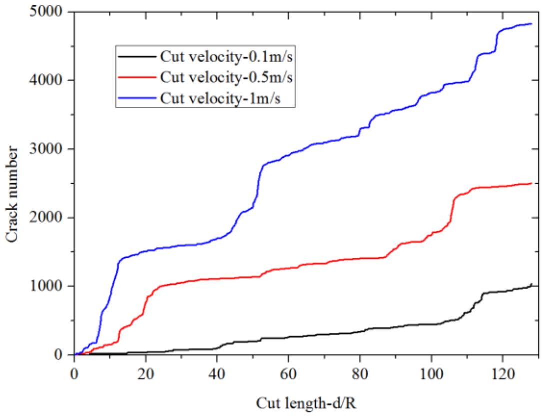

Fig. 21 Crack number versus cut length under hydrostatic pressure with various cutting velocity

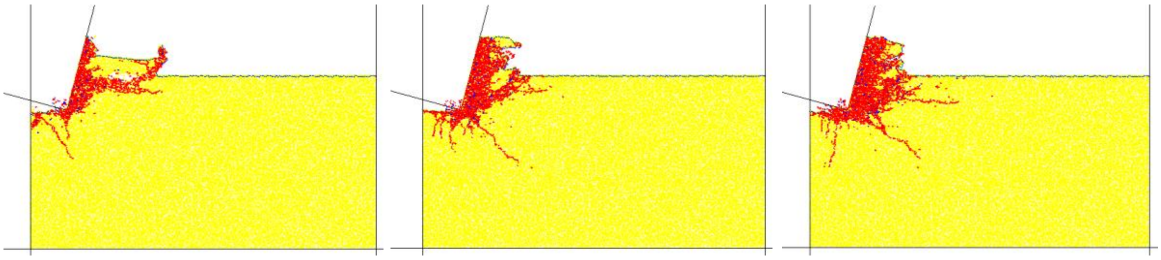

(a) Back rake angle=15° (b) Back rake angle=25° (c) Back rake angle=35°

Fig. 22 The rock cutting failure mechanism with different rake angles of cutter

7. The effect of back rake angle on rock cutting

The effect of back rake angle of cutter on rock failure mechanism is shown in Fig. 22. The results show that the development of horizontal fracture is restricted as the back-rake angle increases. The crack initiates and propagates parallel to the free surface with a smaller rake angle, but with the rake angle increases, the direction of crack initiation and propagation is changed towards into the intact rock. The cutting force of the three conditions are 129 kN/m, 156 kN/m, 205 kN/m respectively, it shows that larger rake angle causes a larger cutting force.

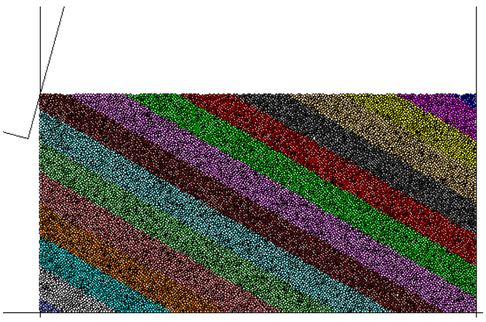

Fig. 23 The schematic of rock sample with joint set

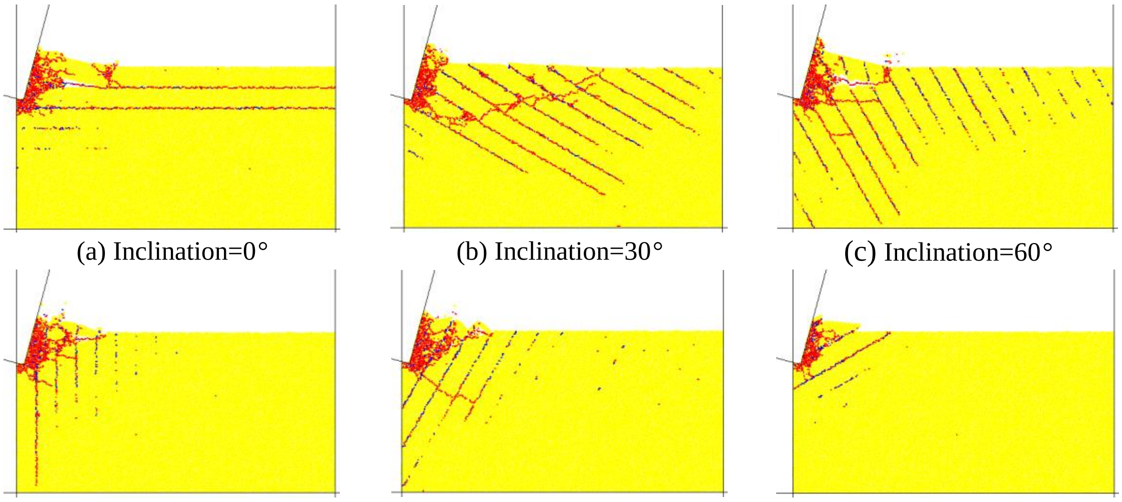

(a) Inclination=0° (b) Inclination=30° (c) Inclination=60°

(d) Inclination=90° (e) Inclination=120° (f) Inclination=150°

Fig. 24 The rock cutting failure mechanism with different inclination angles of joint set

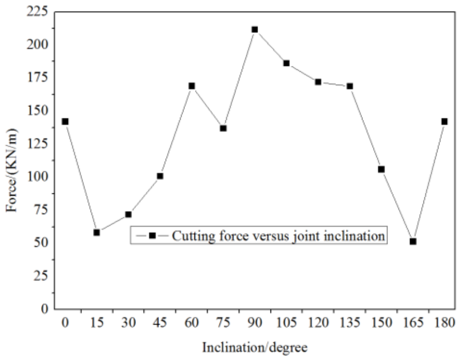

Fig. 25 The cutting force versus inclination angle

8. The effect of joint set on rock cutting

In the prior researches, the rock mass is simply treated as an isotropic material; this method may be acceptable for the shallow formations, but for the deep formations, the anisotropic properties of rock mass become stronger due to the existence of joint sets or fracture plane with the increase of drilling depth. The rock simple with joints which distributed with various inclination angles are established by PFC2D, see Fig. 23. Rock formations are distinguished by various colors. The bond strength of two adjacent formations is defined by the shear and normal bond strength of the contact particles. In general, the bond strength of the joint is much lower than the rock mass, therefore, set the normal and shear bond strength both equal to 10 MPa and the friction is 0.25 in this paper.

The rock cutting failure mechanisms are investigated with different inclination angles of joint, see Fig. 24. The results suggest that the existence of joint have significant influence on crack initiation and propagation, it makes the crack prone to propagate along the joint. The average cutting forces with different inclination angles of joint are shown in Fig. 25; the results indicate that the cutting force reaches to the maximum value while the inclination angle is 90° and decreases to the minimum when the inclination angle is 165°.

9. Conclusions

In this paper, an attempt was made to research the factors influence the failure mechanism based on discrete element method (DEM). The influences of cutting depth, hydrostatic pressure, cutting velocity, back rake angle and joint set on failure mechanism in rock-cutting are researched by PFC2D. The results of this investigation revealed the following findings.

• The ductile failure occurs at shallow cutting depths, characterized by a continuous plastic flow of crushed materials ahead of the cutting tool. The brittle failure occurs while the cutting depth increases beyond a threshold value, characterized by the initiation and propagation of macroscopic cracks along the horizontal direction. The mean forces should have a linear related to the cutting depth if the cutting action is dominated by the ductile mode. However, the mean cutting forces tend to deviate from the linear relationship while the brittle mode is dominated.

• Comparing the fracture evolution mode with no hydrostatic pressure, it can be easily noticed that hydrostatic pressure could significantly influence the fracture evolution, inhibiting the formation of the long horizontal fracture. The failure mechanism changes from brittle mode with larger chips under atmospheric conditions, to ductile mode with crushed chips under hydrostatic conditions. In the hydrostatic pressure case, even the cutting depth is d=53R, the failure mode is still dominated by ductile failure, the mean cutting forces keep increasing linearly until d=53R or even larger. The larger cutting depths cases are not calculated in this paper.

• The influence of velocity on failure mode transition in rock cutting is obviously; the failure mode transition from brittle mode to ductile mode with the cutting velocity increases. As the cutting velocity increases, a grow number of micro-cracks are initiated around the cutter and the volume of the chipped fragmentation is decreasing correspondingly.

• The crack initiates and propagates parallel to the free surface with a smaller rake angle, but with the rake angle increases, the direction of crack initiation and propagation is changed to towards the intact rock; larger rake angle causes a larger cutting force. The existence of joint have significant influence on crack initiation and propagation, it makes the crack prone to propagate along the joint. The average cutting force reaches to the maximum value while the inclination angle is 90° and decreases to the minimum when the inclination angle is 165°.

Acknowledgments

This study is supported by the National Natural Science Foundation of China (Grant No.51674214), International Cooperation Project of Sichuan Science and Technology Plan (2016HH0008), Youth Science and Technology Innovation Research Team of Sichuan Province (2014TD0025). Such supports are greatly appreciated by the authors.

References

Block, G. and Jin, H. (2009), “Role of failure mode on rock cutting dynamics”, *Proceedings of the SPE*

Annual Technical Conference and Exhibition, New Orleans, Louisiana, U.S.A., October.

Che, D., Han, P., Peng, B. and Ehmann, K.F. (2014), "Finite element study on chip formation and force response in two-dimensional orthogonal cutting of rock", *Proceedings of the ASME 2014 International Manufacturing Science and Engineering Conference collocated with the JSME 2014 International Conference on Materials and Processing and the 42nd North American Manufacturing Research Conference*, Detroit, Michigan, U.S.A., June.

Cho, N., Martin, C.D. and Sego, D.C. (2007), "A clumped particle model for rock", *J. Rock Mech. Min. Sci.*, **44**(7), 997-1010.

Cundall, P.A. and Hart, R.D. (1985), *Development of Generalized 2-D and 3-D Distinct Element Programs for Modeling Jointed Rock*, Itasca Consulting Group Inc., Minneapolis, Minnesota, U.S.A.

Cundall, P.A. and Potyondy, D.O. (2004), "A bonded-particle model for rock", *J. Rock Mech. Min. Sci.*, **44**(5), 1329-1364.

Da Fontoura, S.A.B., Inoue, N., Martinez, I.M.R., Cogollo, C. and Curry, D.A. (2012), "Rock mechanics aspects of drill bit rock interaction", *Proceedings of the 12th International Congress on Rock Mechanics*, Beijing, China, October.

Diederich, M.S. (2000), "Instability of hard rock masses: The role of tensile damage and relaxation", Ph.D. Dissertation, University of Waterloo, Waterloo, Canada.

Fang, Z. and Harrison, J.P. (2002), "Application of a local degradation model to the analysis of brittle fracture of laboratory scale rock specimens under triaxial conditions", *J. Rock Mech. Min. Sci.*, **39**(4), 459-476.

Franca, L.F.P. and Lamine, E. (2010), "Cutting action of impregnated diamond segments: Modelling and experimental validation", *Proceedings the 44th US Rock Mechanics Symposium and 5th US-Canada Symposium*, Salt Lake City, Utah, U.S.A., June.

Ghazvinian, E., Diederichs, M.S. and Quey, R. (2014), "3D random Voronoi grain-based models for simulation of brittle rock damage and fabric-guided micro-fracturing", *J. Rock Mech. Geotech. Eng.*, **6**(6), 506-521.

He, X. and Xu, C. (2015), "Discrete element modelling of rock cutting: from ductile to brittle transition", *J. Numer. Anal. Met. Geomech.*, **39**(12), 1331-1351.

Hoover, W.G., Groot, A.J.D., Hoover, C.G., Stowers, I.F., Holian, B.L., Boku, T., Ihara, S. and Belak, J. (1990), "Large-scale elastic-plastic indentation simulations via nonequilibrium molecular dynamics", *Phys. Rev. A*, **42**(10), 5844-5853.

Huang, H., Detournay, E. and Bellier, B. (1999), "Discrete element modelling of rock cutting", *Rock. Mech. Industr.*, **1**(1), 123-130.

Huang, H., Lecampion, B. and Detournay, E. (2013), "Discrete element modeling of tool-rock interaction I: Rock cutting", *J. Numer. Anal. Met. Geomech.*, **37**(13), 1913-1929.

Innaurato, N., Oggeri, C., Oreste, P.P. and Vinai, R. (2007), "Experimental and numerical studies on rock breaking with TBM tools under high stress confinement", *Rock Mech. Rock Eng.*, **40**(5), 429-451.

Itasca, C.G. (2002), *Users' Manual for Particle Flow Code in 2 Dimensions (PFC2D)*, Minneapolis Minnesota, U.S.A.

Jia, L., Chen, M., Zhang, W., Xu, T., Zhou, Y., Hou, B. and Jin, Y. (2013), "Experimental study and numerical modeling of brittle fracture of carbonate rock under uniaxial compression", *Mech. Res. Commun.*, **50**, 58-62.

Ledgerwood, L.W. (2007), "PFC modeling of rock cutting under high pressure conditions", *Proceedings of the 1st Canada-US Rock Mechanics Symposium*, Vancouver, Canada, May.

Lei, S.T. and Kaitkay, P. (2003), "Distinct elementmodeling of rock cutting under hydrostatic pressure", *Key Eng. Mater.*, 250, 110-117.

Mahabadi, O.K., Lisjak, A., Munjiza, A. and Grasselli, G. (2012), "Y-Geo: A new combined finite discrete element numerical code for geomechanical applications", *J. Geomech.*, **12**(6), 676-688.

Mendoza, J.A., Gamwo, I.K., Zhang, W. and Lin, J.S. (2010), "Discrete element modeling of rock cutting usng crushable particles", *Proceedings of the 44th U.S. Rock Mechanics Symposium and 5th U.S.-Canada Rock Mechanics Symposium*, Salt Lake City, Utah, U.S.A., June.

Mendoza, J.A., Gamwo, I.K., Zhang, W. and Lin, J.S. (2011), "Considerations for discrete modeling of rock cutting", *Proceedings of the 45th U.S. Rock Mechanics/Geomechanics Symposium*, San Francisco, California, U.S.A., June.

Menezes, P.L., Lovell, M.R., Avdeev, I.V. and Higgs, C.F. (2014), "Studies on the formation of discontinuous rock fragments during cutting operation", *J. Rock Mech. Min. Sci.*, **71**, 131-142.

Menezes, P.L., Lovell, M.R., Avdeev, I.V., Lin, J.S. and Higgs, C.F. (2014), "Studies on the formation of discontinuous chips during rock cutting using an explicit finite element model", *J. Adv. Manuf. Technol.*, **70**(1-4), 635-648.

Onate, E. and Rojek, J. (2004) "Combination of discrete element and finite element methods for dynamic analysis of geomechanics problems", *Comput. Met. Appl. Mech. Eng.*, **193**(27), 3087-3128.

Richard, T. (1999), "Determination of rock strength from cutting tests", M.Sc. Dissertaion, University of Minnesota, Minnesota, U.S.A.

Richard, T., Detournay, E., Drescher, A., Nicodeme, P. and Fourmaintraux, D. (1998), "The scratch test as a means to measure strength of sedimentary rocks", Proceedings of the *SPE/ISRM Rock Mechanics in Petroleum Engineering*, Trondheim, Norway, July.

Rojek, J., Onate, E., Labra, C. and Kargl, H. (2011), "Discrete element simulation of rock cutting", *J. Rock Mech. Min. Sci.*, **48**(6), 996-1010.

Shimada, S. and Ikawa, N. (1998), *Molecular Dynamics Analysis of Nanometric Metal Cutting Mechanism*, Springer, Berlin, Germany, 63-75.

Stavropoulou, M. (2006), "Modeling of small-diameter rotary drilling tests on marbles", *J. Rock Mech. Min. Sci.*, **43**(7),1034-1051.

Su, O., and Akcin, N.A. (2011), "Numerical simulation of rock cutting using the discrete element method", *J. Rock Mech. Min. Sci.*, **48**(3), 434-442.

Tan, Q., Xu, Z., Xia, Y., Li, J.F., Zhu, Y. and Liu, C. (2013), "Numerical simulation of dynamic response mechanism of rock by shield machine cutters", *Chin. J. Geotech. Eng.*, **35**(2), 235-242.

Xu, W.J., Li, C.Q. and Zhang, H.Y. (2015), "DEM analyses of the mechanical behavior of soil and soil-rock mixture via the 3D direct shear test", *Geomech. Eng.*, **9**(6), 815-827.

CC